Leak-free integrated microfluidic channel fabrication for surface plasmon resonance applications

M-T Bakouche, S Ganesan, David Guérin, D. Hourlier-Bahloul, M Bouazaoui, Jean-Pierre Vilcot, Sophie Maricot

Leak-free integrated microfluidic channel fabrication for surface plasmon resonance applications

Leak-free integrated microfluidic channel fabrication for surface plasmon resonance applications

M-T Bakouche[1] , **S Ganesan**[1], **D Guérin**[1] , **D Hourlier**[1] , **M Bouazaoui**[2], **J-P Vilcot**[1] and **S Maricot**[1]

[1] University Lille, CNRS, Centrale Lille, Yncréa ISEN, Univ. Polytechnique Hauts-de-France, UMR 8520 - IEMN, F-59000, Lille, France
[2] Univ-Lille, CNRS, UMR8523-PhLAM-Physique des Lasers Atomes et Molécules, CERLA/IRCICA, F-59000, Lille, France

E-mail: mbakouche@univ-lille.fr

Abstract

In this paper, we describe a novel fabrication method of a microfluidic integrated surface plasmon resonance (SPR) gold chip based on a (3-mercaptopropyl) trimethoxy silane (MPTMS) self-assembled monolayer. This monolayer was formed at the surface of a microfluidic chip made of polydimethylsiloxane (PDMS). Its presence was confirmed by contact angle and Fourier transform infrared spectroscopy measurements on the modified PDMS surface. A basic, but nevertheless appropriate, 4-channel microfluidic system was made on PDMS and reported on a gold SPR sensor. Sealing tests were carried-out by injecting continuous flows of solutions under gradient pressure up to 1.8 bar. Bonding strength of chemical and corona binding were measured and compared. The test of the integrated microfluidic SPR sensor on an SPR bench validated its functionality and proved as well that no leakage is observed between the different microfluidic channels.

Supplementary material for this article is available online

(Some figures may appear in colour only in the online journal)

1. Introduction

Currently, sensors based on surface plasmon resonance (SPR) physical phenomenon are among the sensors exhibiting the highest sensitivity in material permittivity measurements which one of the main adaptations concerns molecular interaction analysis [1–3]. When those sensors are converted to biosensors using mainly surface chemistry, the SPR detection scheme awards for itself label-free, real-time and extreme kinetics qualifiers that are none the less advantages compared to other molecular interaction detection techniques. Kinetics up to $10^9 \, M^{-1} \, s^{-1}$ and down to $10^{-5} \, M^{-1} \, s^{-1}$ for, respectively, association and dissociation rate values have been recorded [4] as well as an antibody detectivity level as low as $30 \, ng \, ml^{-1}$ [5].

Right now, SPR measurement is usually done launching a SPR sensor into an equipment handling the pressure-contact microfluidic system allowing the sensor to be fed with the ad-hoc solutions, whether reference, functionalization, or under investigation. Prior to use, biologists functionalize the SPR sensors on the measurement equipment following the request of their analyses. After measurements, sensors follow a regeneration protocol in order to be used again.

In the minds building a fully ready-to-use and single-use SPR sensor by embedding the right microfluidic system is still a great challenge. It will allow an initial functionalization of SPR sensors before use and hence greatly simplify the analysis process since only reference and under investigation solutions shall then be launched to conduct analyses.

Polymer-based microfluidic systems using polydimethylsiloxane (PDMS) are increasingly used since the 1990s for the design and the development of lab-on chips, point of care devices and all types of fluidic based sensors [6]. Their fabrication technology is now well known [7]. PDMS can then be considered as the reference material due to its biocompatibility and inertness properties towards biological materials, permeability, flexibility, non-toxicity and easiness in handling. Moreover, it also affords optical transparency in the visible spectrum that is always an asset for experiment monitoring. Beyond that, it offers a wide range of solutions for a cost-less price [8–10]. Thanks to its intrinsic properties, this material adheres easily on silicon-based surfaces such as silicon or glass. Nevertheless, quite often there is a need of plasma treatment to refine the adhesion.

Our first experiments used then an almost usual way making PDMS to adhere on glass substrates that is a plasma, so-called corona treatment [11, 12]. Fairly predictably, PDMS turned out to finely attach on glass. However, plasmonic measurements exhibited noisy responses that result from the observable damage of the plasmonic (gold) layer due to the plasma treatment.

2. SPR sensor and fluidic chip fabrication

As previously mentioned, a rather usual way insuring the PDMS-glass bonding is using corona treatment. Making the SPR detection zones requires then to pattern them under a geometry which shall be smaller to the one of the PDMS fluidic channels (figure 1 (a)); PDMS is then only contacting glass. Lithography and lift-off technique are used to define the patterns of the detection zones. As a result, PDMS is nicely attaching to glass but the thin 35 nm gold film corresponding to the SPR detection zones appears to be damaged due to the plasma treatment. This strongly limits the utility of this plasma corona discharge technique for such a use.

To avoid this plasma treatment, a chemical way can be used to attach PDMS directly on gold surface. 11-mercaptoundecanoic acid (11-MUA) and aminopropyl trimethoxysilane (APTMS) self-assembled monolayers were respectively anchored on gold and PDMS surfaces by Ouellet et al [9]. Both were cross-linked using 1-ethyl-3-(3-dimethylaminopropyl) carbodiimide/N-hydroxysuccinimide
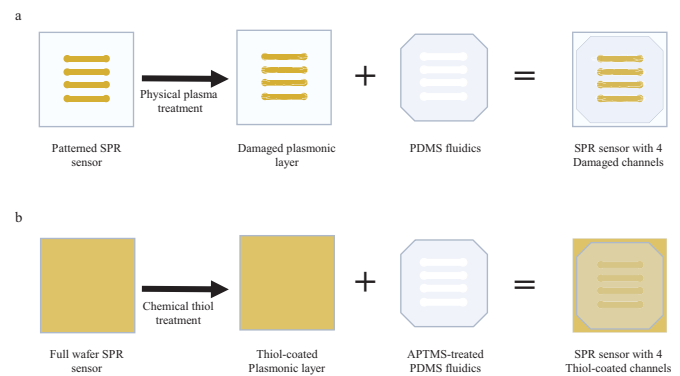

Figure 1. (a) Physical process; (b) chemical process.

(EDC/NHS) as amine-coupling agents before mutual adhesion (figure 1(b)). This technique displayed too nice PDMS to gold bonding but SPR channels are then coated with the 11-MUA monolayer that can turn out to be inconvenient for further physico-chemistry processes on the SPR channels. Although an exhaustive list of PDMS-bonding strategies on different surfaces for multiple applications is cited in [9], few were used for SPR biosensors fabrication and none reports on the stability of the microfluidic assembly. We present hereby a technique used by Byun *et al* [13] that is based on silanated thiol-gold bonding process and cumulates the advantages of both physical and chemical techniques, i.e. undamaged and chemically clean SPR channels. The fluidic integrated SPR sensor is made of two separate parts, the SPR sensor and the fluidic circuitry, that are assembled thereafter.

2.1. SPR sensor fabrication

The employed SPR test set-up works in the near infra-red optical domain (1550 nm) and uses an HZF-1 (n = 1.62 @ 1550 nm) prism [14]. Same material is hereby used for the fabrication of the sensors in order to avoid optical reflection at the prism-sensor interface. Obviously, the technique hereafter reported can be used on any glass substrate since none of its parameters is directly involved in the fabrication process.

The SPR sensor surface is made of a Ti/Au (2 nm/35 nm) layer (Ti acts as an adhesion layer) deposited by e-beam evaporation on 25×25 mm HZF-1 slides. These slides are cleaned in a piranha solution (75% H_2SO_4 + 25% H_2O_2) prior metallization. The metallization is made all over the surface area of the sensor.

2.2. Fluidic chip fabrication

Sylgard™184 silicon elastomer and curing agent were purchased from Dow®. (3-Mercaptopropyl trimethoxysilane) was bought from Sigma-Aldrich and absolute ethanol was obtained from Carlo-Erba. SU-8 2035 and 2075 photoresists were purchased from Kayaku advanced materials™. All reagents are of analytical grade and used as provided without any further purification.

The PDMS base solution is prepared by mixing the silicone elastomer and its curing agent with a 10:1 weight ratio

as recommended by the manufacturer. This mixture is poured into a petri dish containing a mold made of SU-8 photoresist patterns fabricated on a silicon wafer [15, 16]. Prior to PDMS casting, this mold is Teflon-like-coated using C_4F_8 plasma treatment in order to facilitate the mold release. For the demonstration, the patterns corresponding to the microfluidic circuitry consists of four microchannels with dimensions of $10 \times 1.5 \times 0.2$ mm (L × W × H). Once the mold is filled, PDMS is cured at 70 °C for 1 h. Release is made with a cutter blade separating PDMS from the petri dish and by hand stripping PDMS from the SU-8 patterned silicon mold.

At this stage, the two parts of the sensor, SPR sensor and microfluidic chip, are separately available and ready to be assembled together to form the integrated fluidic sensor.

2.3. Processing of fluidic chip towards integration

The principle of sensor integration is based on a (3-mercaptopropyl) trimethyloxane (MPTMS) self-assembly process. We have chosen a thiolated-silane linker as MPTMS since it is well known that thiolated-molecules strongly bind to gold surfaces. During the PDMS treatment, the silane forms a self-assembled monolayer on PDMS, then bonds covalently to gold via its -SH groups. The strong Au-S bond energy about 298 ± 2 kJ mol^{-1} and its length of 2.156 Å [17] should provide of a good sealing of PDMS fluidic chip onto gold SPR layer.

Hence, PDMS surface preparation is needed before assembling the integrated fluidic sensor. The PDMS chip surface firstly goes through a UV-O_3 treatment for 5 min in order to generate a thin layer of hydroxyl groups able to accommodate chemical reactions [18]. It is then immersed in an ethanoic solution of MPTMS at a volume ratio of 50:1 for 1 h. The PDMS chip is eventually rinsed three times with ethanol, then with deionized water so that non-grafted MPTMS molecules are eliminated (see supplementary materials at (stacks.iop.org/JMM/30/125003/mmedia).

Before assembling, the PDMS chip surface is characterized in order to validate the surface modification brought by the MPTMS treatment. Contact angle goniometry (GBX Digidrop equipment) is used as an usual tool characterizing wettability of surfaces. As an additional and prominent surface characterization method, attenuated transmittance reflection-Fourier transform infrared spectroscopy (ATR-FTIR) measurements have been employed to investigate the MPTMS self-assembled monolayer formation on the PDMS surface. A Perkin-Elmer Spectrum GX spectrometer equipped with a Specac Goldengate ATR instrument fitted with a germanium crystal is used. Both UV-O_3 and MPTMS treated PDMS surfaces were analyzed. Their respective spectra in the 4000–400 cm^{-1} spectrum range were collected by averaging 50 succeeding measurements, then post-treated using KnowItAll® software by applying an automated ATR-correction, followed by a baseline correction and finally a normalization.

3. Surface characterization

3.1. Contact angle goniometry

The GBX Digidrop instrument is semi-automated and relies on image data processing of a liquid drop on a solid surface. Its contact angle accuracy is ±0.07°. Since the wettability phenomenon is temperature-dependent, experiment temperature is controlled. A 2 μl drop of deionized water is deposited on the sample, here PDMS, surface at 20 °C and the angle is measured using both the instrument's proprietary software and ImageJ. The three-phase intersect method is employed for the measurement [19].

Figure 2 shows contact angle measurements for both UV-O_3 and MPTMS modified PDMS surfaces. UV-O_3-treated PDMS showed a contact angle of 102° which is typical for a hydrophobic surface, meanwhile MPTMS-treated surface displayed a hydrophilic nature with a typical value of 74° [20].

The decrease in contact angle value from 102° for the UV-O_3 treated surface down to 74° for the MPTMS-modified one reveals the MPTMS self-assembled monolayer (SAM) formation on the PDMS surface. This result comes in accordance with other MPTMS-SAM formation studies on silicon-based surfaces, proposing a well-organized self-assembled monolayer with an up-oriented thiol group [20, 21].

3.2. ATR-FTIR

Table 1 shows the most characteristic IR bands of both MPTMS-modified and UV-O_3 PDMS material. Figure 3 shows spectra of both UV-O_3 and MPTMS modified PDMS surfaces.

MPTMS modified-PDMS showed peaks at 789 cm^{-1} and 844 cm^{-1} that are assigned to the -CH3 rocking vibrations and ν-Si-C symmetric stretching vibrations, respectively. In addition, v-Si-O-Si asymmetric stretching vibrations are recorded at 1012 cm^{-1}; they are present inside the PDMS matrix and at its surface after MPTMS anchoring. Furthermore, the presence of methyl groups in the PDMS matrix was confirmed by the intense narrow peak at 1258 cm^{-1} and the peaks at 2905 and 2963 cm^{-1} that correspond to the –CH3 asymmetric bending, symmetric and asymmetric stretching vibration modes respectively. In addition, a broad band at 1414 cm^{-1} is observed, it corresponds to CH2 = CH2 scissors vibrations.

In addition to the previously observed peaks of the typical vibrational modes, weak broad bands at 1726 cm^{-1} and at 3277 cm^{-1} are observed only on the UV-O_3 activated PDMS spectrum corresponding to the carbonyl stretching vibrations and ν-OH symmetric stretching mode respectively [18, 22–24]. The latter is present in the -Si-OH bond and is due to the PDMS surface exposure to UV-O_3 treatment.

Indeed, as illustrated in figure 4, PDMS surface oxidation by UV-O_3 conducts to its degradation and silanol formation
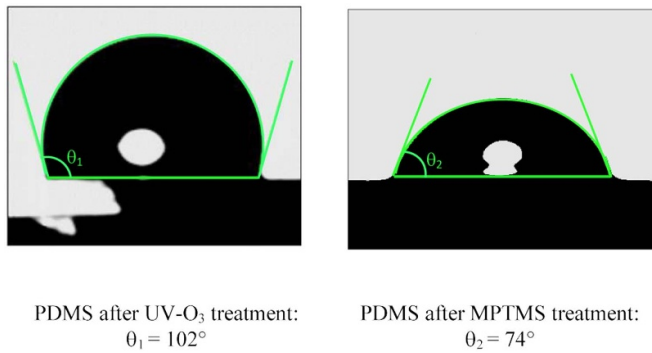
PDMS after UV-O$_3$ treatment:
$\theta_1 = 102°$

PDMS after MPTMS treatment:
$\theta_2 = 74°$

Figure 2. Contact angle measurements of UV-O3 and MPTMS treated PDMS surfaces.

Table 1. Assignment of ATR-IR spectra for both UV-O3 and MPTMS treated PDMS surfaces [18, 22–24].

Peak/band area (cm^{-1})	Vibration mode
789	ρ-CH3 rocking vibrations
844	ν_s-Si-C symmetric stretching vibrations
1012	ν_a-Si-O-Si asymmetric stretching vibrations
1258	σ_a-CH3 asymmetric bending vibrations
1414	CH2=CH2 scissors vibrations
1726	ν-C=O stretching vibrations
2905 and 2963	ν_s-CH3 and νa-CH3 symmetric and asymmetric stretching vibrations
3277	ν_s-OH symmetric stretching vibrations

[25]. As reported in [22], this transformation occurs down to a certain depth according to time exposure under UV-O$_3$. This observation comes in agreement with the presence of –CH3 groups inside the PDMS matrix as the above reported characteristic vibration peaks confirm. We suggest that the ethylene and carbonyl groups formations occur partially at the PDMS surface and are a parallel reaction since UV-O$_3$ treatment shatters PDMS-structure [18]. The disappearing of the wide band around 3200 cm^{-1} after surface modification by MPTMS confirms the mercaptopropyl silane self-assembly on PDMS surface (see figure 5(c)). The joined disappearing of the peak at 1726 cm^{-1} (see insert in figure 3) testifies the SAM formation since MPTMS molecules form Si-O-Si bonds with all the present oxygen at PDMS surface whatever they are in carbonylated or hydroxylated state.

Figure 5 shows the well-known scheme of (3-mercaptopropyl) trimethoxysilane self-assembly on inorganic surfaces. As described in figure 5(a) [26, 27], it is usually proposed that the MPTMS undergoes a hydrolysis of alkoxysilanes, then the hydrolyzed molecules tend to form a polymeric matrix by forming hydrogen bonds which finally conducts to its grafting on the PDMS surface.

We suggest a more detailed reaction mechanism that can occur for the (3-mercaptopropyl) trimethoxysilane grafting on PDMS surface during its prime step which is the MPTMS hydrolysis. Firstly, the lone pair electrons of oxygen that are present in the aqueous medium attack the silicon releasing the labile methoxy group. Secondly, the methanoate moiety grabs the proton attached to the formed oxonium groups so that methanol can be formed. A complete MPTMS hydrolysis leads to (3-mercaptopropyl) silanetriol (MPST) formation (figure 5(a)). Underneath the usual depiction of the reaction that is presented in figure 5(b), we evoke that polycondensation undergoes through a SN2-Si mechanism as discussed in [28] and that it is triggered by lone pair electrons of oxygen of the silanol groups that take a proton from another silanol group in vicinity. Subsequently, this deprotonated silanol group attacks the silicon atom of the protonated silanol releasing a molecule of water and the process is repeated until the MPST oligomer is formed. Finally (figure 5(c)), by the same SN2-Si reaction, the MPST oligomer self-assembles on PDMS surface; lone pair electrons of oxygen of the silanol groups take proton from hydroxyl groups from the UV-O$_3$ treated PDMS surface followed by the attack of the silicon by the deprotonated oxygen releasing so water.

4. Fabrication of the integrated fluidics SPR sensor

It is then time to assemble the MPTMS-treated PDMS chip onto the SPR surface. It is hand-pressed against the gold surface and left under vacuum-annealing for 1 h at 60 °C. This bake ensures a quicker bonding process, since, 24 h are requested at room temperature.

A homogenous and irreversible bonding is so achieved via the Au-S bond (figure 6).

The final integrated fluidic SPR chip is shown in figure 7. At first, the PDMS adhesion has been checked simply by hand pulling on the PDMS. No disbonding was observed. It is worth mentioning that a non-treated PDMS chip would have detached easily.

5. Mechanical test

Tensile strength test was performed on a Mecmesin MultiTest 2.5-*d* instrument for both classical corona-discharge treated and chemically bonded samples (figure 8). The corona bonding was realized by treating both clean glass and PDMS surfaces with corona discharge for 2 min using a handheld BD-20AC Corona treater device, then treated glass and PDMS were aligned and attached together. The assembly was then kept at 80 °C overnight to obtain a perfect bonding. The chemically bonded sample was made using the process above mentioned.

The samples shown in figure 8(a) were of 25 × 75 mm dimensions having bonded PDMS on extremities. Those were secured by jaws in the tensile strength measurement equipment to ensure uniform pressure distribution. Cross-head velocity was 10 mm min^{-1} and tensiometer data were recorded using the embedded equipment software (figure 8(b)).

Figure 9 shows obtained curves of force versus elongation. Both chemically and corona-discharge bonded samples exhibit the same linear behavior under elongation. They also present
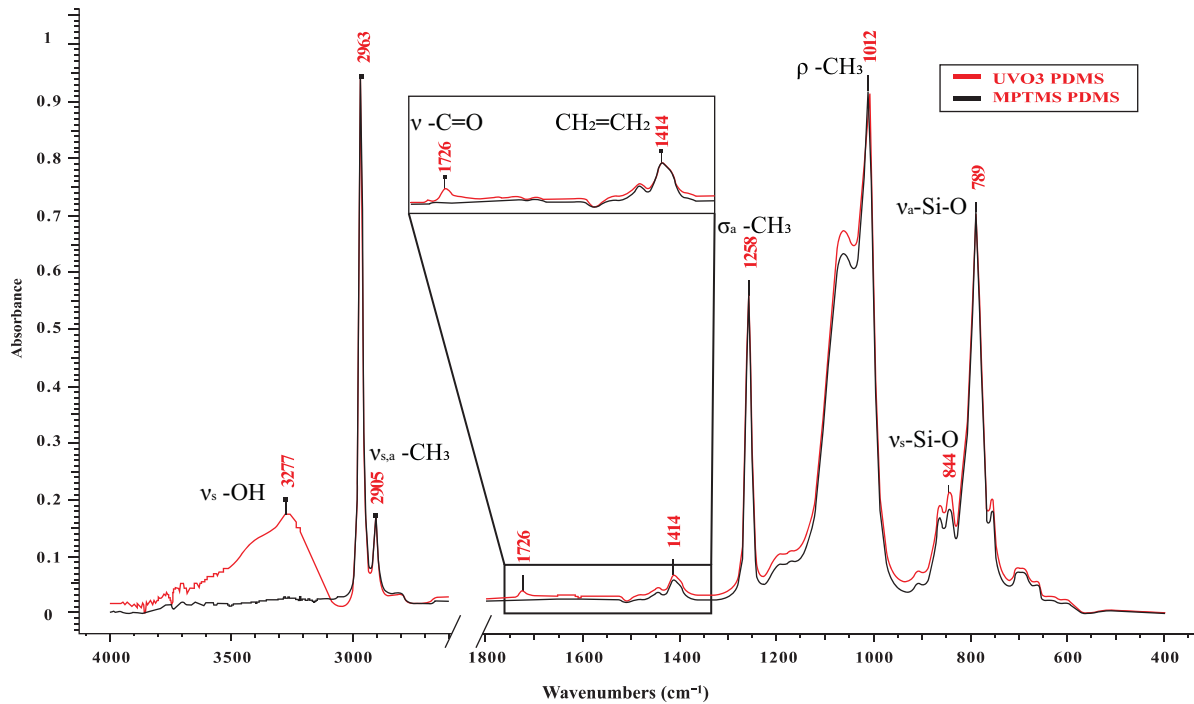
Figure 3. Normalized ATR-FTIR spectra of UV-O3 and MPTMS treated PDMS surfaces.
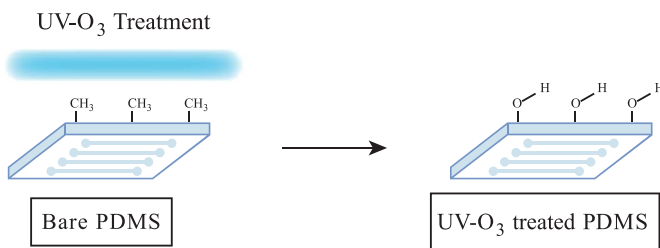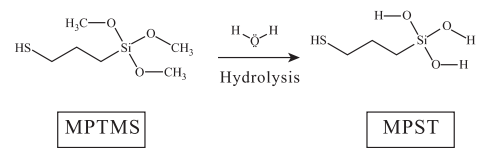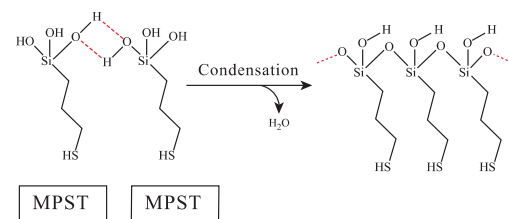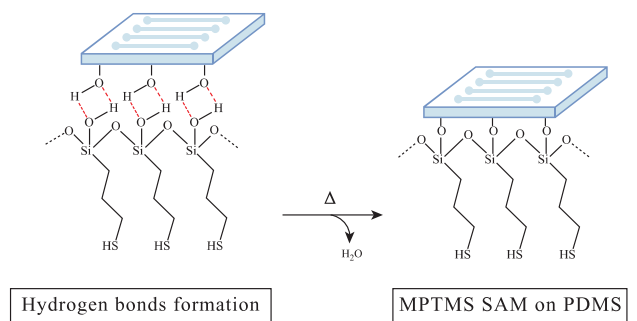

Figure 4. PDMS surface modification by UV-ozone

the same elongation at failure of 20 mm corresponding to a strain $\varepsilon = 1.6$ that agrees with data reported by Johnston *et al* [29]. However, the average failure load (break point) of chemically bonded sample is 30% higher indicating that this sample is stiffer than the corona-discharge bonded one.

6. Integrated fluidic SPR sensor test

The sensor was tested first under visual inspection using an ink circulation and second on the SPR set-up.

The microfluidic channels are fed using a 1/16″ OD x 0.51 mm ID Tygon tubing. Tubing is inserted into the PDMS above the input/output reservoirs located at both ends of each microfluidic channel and sealed with annealed liquid PDMS to avoid any unwanted fluidic leakage.
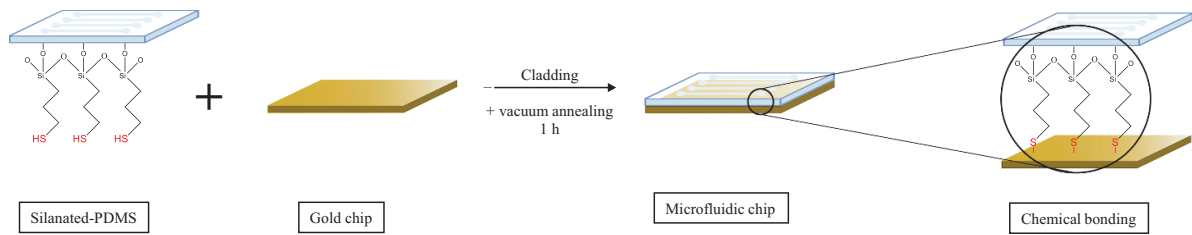

Figure 5. Reactional mechanism of MPTMS self-assembly on PDMS [24, 25].

Figure 6. Bonding process of MPTMS-treated PDMS onto a SPR gold chip.
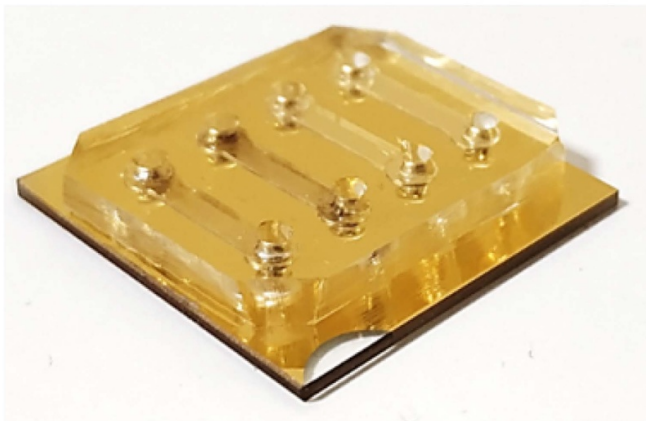

Figure 7. Final aspect of the integrated microfluidic SPR sensor. PDMS microfluidic channels are seen in transparency.

6.1. Ink test

Microfluidic system sealing has been tested by injecting a black ink solution in the four microfluidic channels continuously during 5 min through a pressure gradient up to 1.8 bar using an Elveflow™ OB1 pressure pump, then observing the chip state under optical microscope.

This process was made five times on a same chip and repeated on three different sensors.

Figure 10 illustrates the microfluidic integrated SPR chip under and after ink injection. Figures 10(a) and 10(b) show channel filling while operating the ink test at, respectively, half and full length. Naked-eye observations of the four channels after filling show neither inter-channels nor outer leaks (figure 10(c)). Besides the static views presented hereby, no leaks have been observed during full testing time whatever the flow rate was. An advanced observation using optical microscope (figure 10(d)) confirmed the leak-free microfluidic circuitry with a clear boundary for microfluidic channels. This result confirms the chemical-bonding strength by using MPTMS as a linker and that the formed SAM is uniform and continuous.

6.2. SPR test

As a functional test but also as a sealing test, SPR experiments were conducted. Owing to the intrinsic low penetration depth (some hundreds of nanometers) of the plasmonic wave, SPR measurement is also particularly well suited to detect any leak
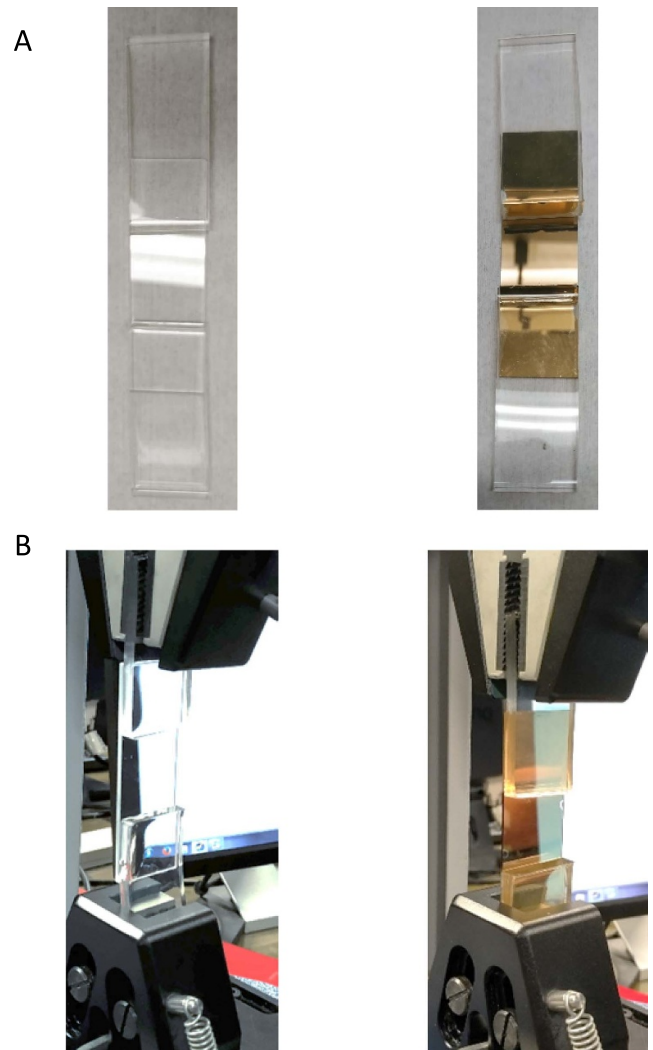

Figure 8. (A) Corona-discharge bonded sample (left) and chemically bonded sample (right). (B) Samples under respective tensile strength test.

that could exist on chip surface, i.e. to spot any irregularity in the PDMS to gold sealing process. The SPR experimental set-up is based on an angular interrogation scheme [14]. The result is observed through the plasmonic amplitude response obtained as an image on an InGaAs short wave infrared camera from Photonic Science. Here the test fluids consist of ethylene glycol-based solution presenting a refractive index. The fluidic experiment has been made at the same flow rates that have been used for the ink test. In order to validate the stability of the
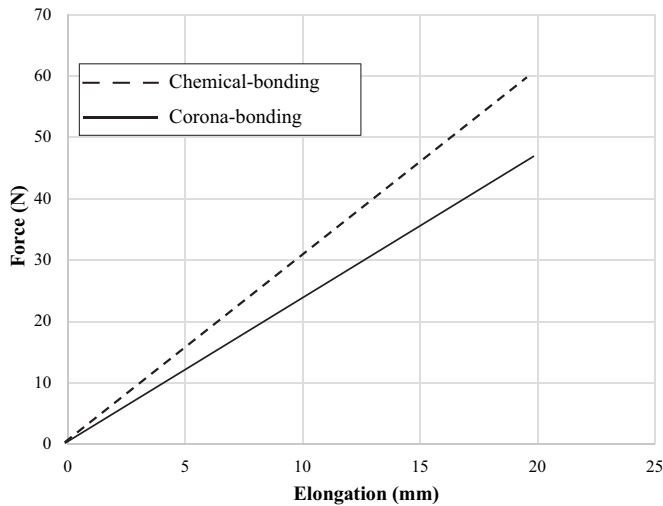
Figure 9. Tensile strength curves for corona-discharge (solid line) and chemically (dashed line) bonded PDMS samples.
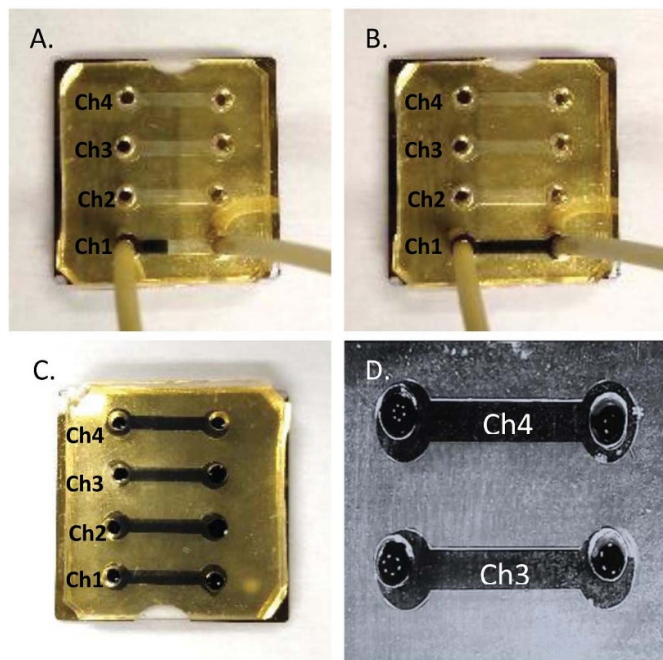

Figure 10. (A) Halfway filling of one channel, (B) full filling of one channel, (C) all channels filled, (D) zoom under optical microscope on 2 filled channels.

bonding process, the experiment duration has been extended up to 20 min without any appearance of leak.

Figure 11 depicts a plasmon profile comparison observed on both corona-discharge (solid-line) and chemically (dashed-line) treated microfluidic chips. The corona-bonded sample exhibit a wider plasmonic response than the chemically bonded one; for example, at 0.3 normalized intensity value, respective full-width at half maximum (FWHM) are 0.48° and 0.32°. This higher FWHM value for corona-discharge treated sample illustrates the gold surface degradation under the corona surface treatment. Indeed, a lower FWHM value improves the raw signal integrity and its post-processing [30].
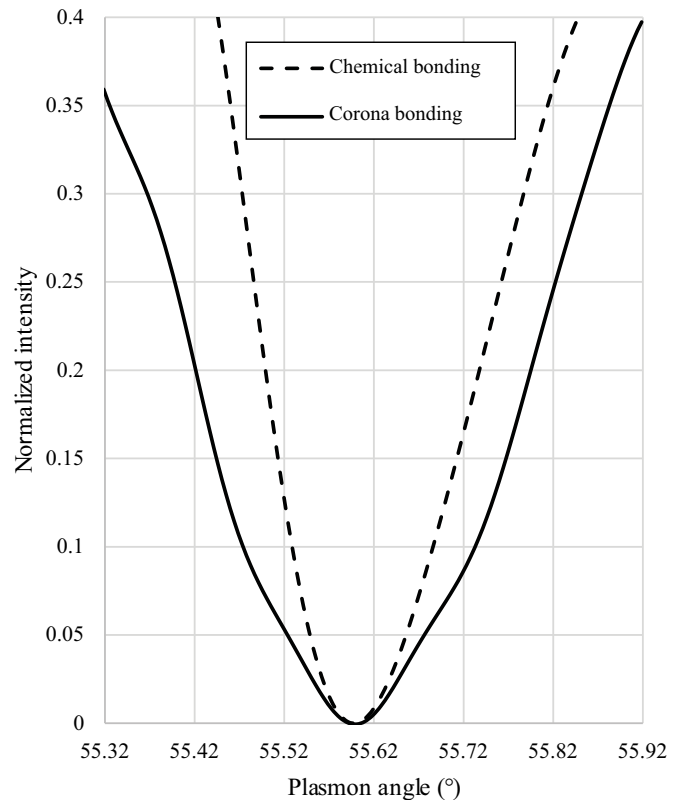

Figure 11. Normalized plasmonic response profile for both corona and chemically bonded samples.

7. Conclusion

In conclusion, we have demonstrated that leak-free integrated microfluidic SPR sensors can be fabricated using a (3-mercaptopropyl) trimethyloxane (MPTMS) self-assembly process. To achieve the bonding, the PDMS microfluidic chip is UV-O_3 and MPTMS treated prior to its attachment to the gold surface. A comparison between corona-discharge and chemically bonded PDMS samples using tensile strength measurements shows that the latter one is more rigid. Moreover, visual as well as SPR tests have been conducted under pressurized fluidic injection insuring that no cross channel, and even any leak occurs. A four-channel PDMS device was successfully prepared and tested on an SPR set-up. Obviously, more complex microfluidic circuitry can be integrated. Such integrated SPR sensors pave the way to the realization of ready to use sensors since, prior to use, each channel could be functionalized in a different way.

Acknowledgments

ORCID iDs

M-T Bakouche ☉ https://orcid.org/0000-0001-7623-5883
D Guérin ☉ https://orcid.org/0000-0002-4338-1742
D Hourlier ☉ https://orcid.org/0000-0002-4044-4429
J-P Vilcot ☉ https://orcid.org/0000-0002-6448-4740
S Maricot ☉ https://orcid.org/0000-0001-8512-0666

References

[1] Bhandari D, Chen F-C, Hamal S and Bridgman R C 2019 *Antibodies* **8** 22
[2] Bocková M, Slabý J, Špringer T and Homola J 2019 *Annu. Rev. Anal. Chem.* **12** 151
[3] Garzón V, Pinacho D G, Bustos R-H, Garzón G and Bustamante S 2019 *Biosensors* **9** 132
[4] Helmerhorst E, Chandler D J, Nussio M and Mamotte C D 2012 *Clin. Biochem. Rev.* **33** 161
[5] Suzuki M, Iribe Y and Tobita T 2008 *Surface Plasmon Resonance Array Devices Handbook of Biosensors and Biochips* (Hoboken, NJ: Wiley)
[6] Azouz A B, Vázquez M and Brabazon D 2014 *Comprehensive Materials Processing* pp 447 (Amsterdam: Elsevier)
[7] Wang D-S and Fan S-K 2016 *Sensors* **16** 1175
[8] Nag A, Feng S, Afsarimanesh N, Mukhopadhyay S and Kosel J 2018 *Proc. of* 12th *Int. Symp. on Medical Information and Communication Technology (ISMICT)* 1–5
[9] Ouellet E, Yang C W T, Lin T, Yang L L and Lagally E T 2010 *Langmuir* **26** 11609–14
[10] Casanova-Moreno J, To J, Yang C W T, Turner R F B, Bizzotto D and Cheung K C 2017 *Sensors Actuators* B **246** 904–9
[11] Wu J and Lee N Y 2014 *Lab on a Chip* **14** 1564–71
[12] Eddings M A, Johnson M A and Gale B K 2008 *J. Micromech. Microeng.* **18** 067001
[13] Byun I, Coleman A W and Kim B 2013 *J. Micromech. Microeng.* **23** 085016
[14] Hottin J, Wijaya E, Hay L, Maricot S, Bouazaoui M and Vilcot J-P 2013 *Plasmonics* **8** 619–24
[15] Natarajan S, Chang-Yen D A and Gale B K 2008 *J. Micromech. Microeng.* **18** 045021
[16] Zhang Z, Zhao P, Xiao G, Watts B R and Xu C 2011 *Biomicrofluidics* **5** 046503
[17] Kokkin D L, Zhang R, Steimle T C, Wyse I A, Pearlman B W and Varberg T D 2015 *J. Phys. Chem. A* Vol. **119** pp 11659–67
[18] Özçam A E, Efimenko K and Genzer J 2014 *Polymer* **55** 3107–19
[19] Faghri A, Zhang Y *et al* 2006 *Transport Phenomena in Multiphase Systems*, (Cambridge, MA: Academic Press) pp 331
[20] Aswal D K, Lenfant S, Guerin D, Yakhmi J V and Vuillaume D 2005 *Nanotechnology* **16** 3064
[21] Chang C-Y, Chang Y-C, Huang W-K, Liao W-C, Wang H, Yeh C,, Tsai B-C, Huang Y-C and Tsao C-S 2016 *J. Mater. Chem.* A **4** 7903–13
[22] Berdichevsky Y, Khandurina J, Guttman A and Lo Y-H 2004 *Sensors Actuators* B **97** 402–8
[23] Mihelčič M, Surca A K, Kreta A and Gaberšček M 2017 *Croat. Chem. Acta.* **90** 169–75
[24] Agrawal N, Low P S, Tan J S J, Fong E W M, Lai Y and Chen Z 2019 *Nano Mater. Sci.* **2** 281–91 in press
[25] Hoang M V 2016 *J. Micromech. Microeng.* **26** 105019
[26] Hermanson G T 2013 *Bioconjugate Techniques* (London: Academic Press)
[27] Arkles B 1977 *Chemtech* **7** 766
[28] Issa A and Luyt A 2019 *Polymers* **11** 537
[29] Johnston I D, McCluskey D K, Tan C K L and Tracey M C 2014 *J. Micromech. Microeng.* **24** 035017
[30] Gupta B D, Shrivastav A M and Usha S P 2017 *Optical Sensors for Biomedical Diagnostics and Environmental Monitoring* (Boca Raton, FL: CRC Press)